Imaging of normal and pathologic joint synovium using nonlinear optical microscopy as a potential diagnostic tool

Nivedan Tiwari
University of California, Irvine
Beckman Laser Institute
1002 Health Sciences Road
Irvine, California 92612

Sanjay Chabra
3943 Irvine Boulevard #335
Irvine, California 92602

Sheherbano Mehdi
23441 Madison Avenue, Suite 340
Torrance, California 90505

Paula Sweet
Tatiana B. Krasieva
University of California, Irvine
Beckman Laser Institute
1002 Health Sciences Road
Irvine, California 92612

Roy Pool
Texas A&M University
College of Veterinary Medicine
Department of Veterinary Pathobiology
College Station, Texas 77843-4467

Brian Andrews
University of Notre Dame Australia
School of Medicine, Fremantle
47 Henry Street (PO Box 1225)
Fremantle, Western Australia 6959

George M. Peavy
University of California, Irvine
Beckman Laser Institute
1002 Health Sciences Road
Irvine, California 92612

Abstract. An estimated 1.3 million people in the United States suffer from rheumatoid arthritis (RA). RA causes profound changes in the synovial membrane of joints, and without early diagnosis and intervention, progresses to permanent alterations in joint structure and function. The purpose of this study is to determine if nonlinear optical microscopy (NLOM) can utilize the natural intrinsic fluorescence properties of tissue to generate images that would allow visualization of the structural and cellular composition of fresh, unfixed normal and pathologic synovial tissue. NLOM is performed on rabbit knee joint synovial samples using 730- and 800-nm excitation wavelengths. Less than 30 mW of excitation power delivered with a 40×, 0.8-NA water immersion objective is sufficient for the visualization of synovial structures to a maximum depth of 70 μm without tissue damage. NLOM imaging of normal and pathologic synovial tissue reveals the cellular structure, synoviocytes, adipocytes, collagen, vascular structures, and differential characteristics of inflammatory infiltrates without requiring tissue processing or staining. Further study to evaluate the ability of NLOM to assess the characteristics of pathologic synovial tissue and its potential role for the management of disease is warranted.
[DOI: 10.1117/1.3484262]

Keywords: laser scanning microscopy; multiphoton microscopy; synovium; rheumatoid arthritis; rabbit.

Paper 10137R received Mar. 17, 2010; revised manuscript received Jul. 6, 2010; accepted for publication Jul. 14, 2010; published online Sep. 13, 2010.

1 Introduction

Current data on the prevalence of arthritis and other rheumatic conditions in the United States has been published recently.[1,2] The most common form of arthritis is osteoarthritis (OA), which affects an estimated 27 million people, with the most common site of OA involvement being the knee joint.[2] Of the population with inflammatory arthritis, rheumatoid arthritis (RA) is estimated at 1.3 million, spondyloarthropathies at between 0.6 to 2.4 million, and gout at 3.0 million. Arthritis can result in irreversible destruction and loss of normal articular cartilage. Accurate and early diagnosis is the key to achieving success in patient management by alleviating symptoms and preserving function early in the course of the disease while reducing progression of joint inflammation and damage before severe joint degeneration occurs.

The synovial membrane is a thin tissue that covers intra-articular surfaces of the fibrous joint capsule[3] [Fig. 1(a)]. It serves as an important source of nutrients and lubricants for

Address all correspondence to: Nivedan Tiwari, University of California, Irvine, Beckman Laser Institute, 1002 Health Sciences Road, Irvine, California 92612. Tel: 949-824-4713; Fax: 949-824-8413. E-mail: ntiwari@uci.edu

1083-3668/2010/15(5)/056001/10/$25.00 © 2010 SPIE

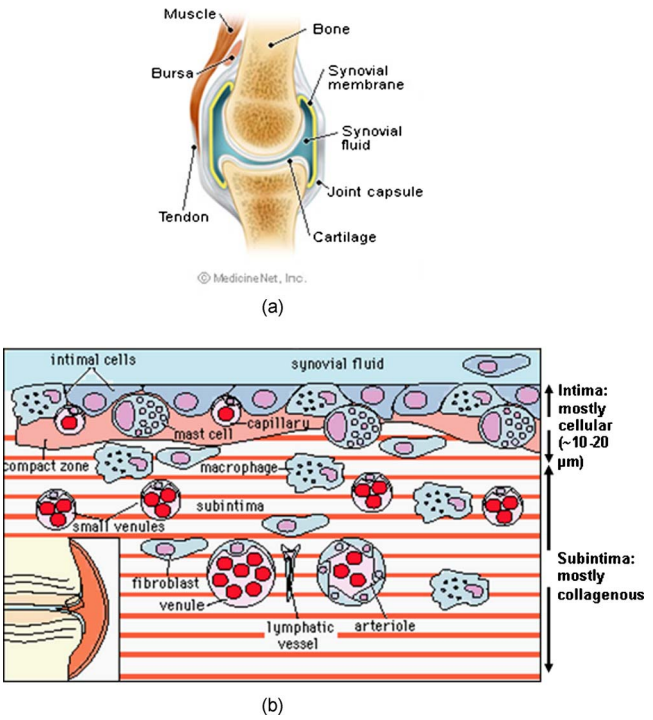

Fig. 1 Schematic depictions of (a) diarthrodial joint structure and (b) the layered structure of synovium.

the joint. The synovium is composed of two regions; the intima (surface layer) and the subintima, a more loosely packed stroma below the intima [Fig. 1(b)].

The normal intima is one to three cells in thickness (10 to 30 μm)[4] and is comprised of bone-marrow-derived macrophages known as type A synoviocytes and fibroblast-like type B synoviocytes. The cells within the intima produce extracellular matrix molecules and mediate the production and clearance of synovial fluid.[4] The type B cells differ from other fibroblast cells in that they exhibit a high activity of uridine diphosphoglucose dehydrogenase and express vascular cell adhesion molecule-1.[5]

Normal intima has a uniform appearance throughout a joint and demonstrates no difference from joint to joint;[6] however, based on characteristics of the subintimal tissue, the synovium is classified into three morphological types, fibrous, areolar, and adipose. The fibrous type is largely composed of collagen fibrils that form fibers and is found where synovium is exposed to pressure.[6] The areolar type is located where the synovial membrane freely moves over the fibrous joint capsule and has fewer collagen fibers but more interfibrillary matrix.[6] The adipose type covers intra-articular fat pads.[7] Combinations of these three basic types occur and are referred to as fibro-areolar and areolar-adipose types.[6]

Human subintima is formed by a loose collagen network containing fibroblasts, adipocytes, macrophages, elastin, mast cells, and blood vessels. Mast cells are absent in rabbit synovium.[6,8] The synovial membrane appears to be free of nerve endings with the exception of autonomic fibers in the adventitia of subintimal blood vessels.[6,8] Capillaries promote rapid nutrient exchange and are usually of the continuous

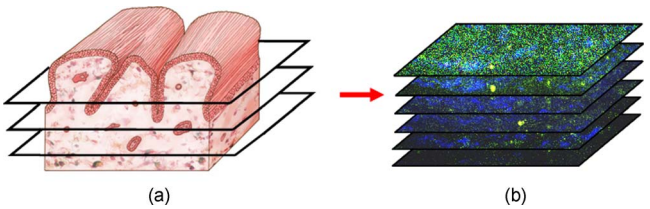

Fig. 2 Schematic depiction of optical sectioning of thick synovial tissue using NLOM. Individual images obtained in tangential planes at specific depth intervals of the tissue (a) can be assembled into a 3-D tomographic stack of images (b) referred to as a Z stack.

type, but can be of the superficial fenestrated type in humans and rabbits.[9]

Nonlinear optical microscopy (NLOM) produces high-resolution structural images using both two-photon fluorescence (TPF) and second harmonic generation (SHG) signals from tissue constituents.[10] The TPF signal is generated when two photons are simultaneously absorbed by fluorophores, such as NADH, riboflavin, folic acid, and retinol, provoking an electronic transition of the fluorophore to an excited state. When the fluorophore returns to its stable state, it emits a single photon producing a detectable signal.[11] The SHG signal is generated by the interaction of intense light with tissue constituents, such as collagen, that have a high nonlinear susceptibility and noncentrosymmetric structure. The SHG signal occurs at exactly half the wavelength of the incident photons.[12]

Wavelengths in the near-infrared region that permit deep penetration into tissues are used as excitation sources for NLOM.[13] TPF and SHG signal generation in NLOM only occurs within the focal volume of a microscope objective where the density of incident photons is very high.[14] This results in photon emissions at the focal point of the imaging beam without the generation of interfering background fluorescence emission from tissue above or below the focal plane of the objective.[15] Scanning along a plane at a fixed focal distance within tissue allows NLOM to optically section and tomographically image thick biological specimens without the need for tissue processing and sectioning (Fig. 2).

The organization of synovium is complex, and alterations in response to various diseases have characteristic histologic changes and profound influences on joint structure and function. Histopathologic changes seen in synovium that are characteristic of RA include: 1. intimal hypertrophy (an increase of eight to ten cells in thickness) due to macrophage influx and some increase in synoviocytes, 2. vascular proliferation, and 3. cellular infiltration of the subintima predominated by mononuclear inflammatory cells (lymphocytes, plasma cells, and macrophages).[16,17] In septic arthritis, as in other forms of nonimmune-mediated inflammatory joint disease, the synovium demonstrates much different pathology with: 1. loss of normal intimal and subintimal morphology, and 2. a predominately polymorphonuclear (neutrophil) inflammatory response with macrophage infiltration and increased fibroblast activity.[18]

Due to limitations of resolution, imaging modalities like MRI and ultrasound provide only a limited assessment of the synovium, resulting in the need for tissue biopsy to visualize and characterize synovial pathology. The limitations of reso-

lution of current imaging technologies for joint disease and the hesitancy to perform invasive biopsy procedures, particularly on a recurring basis to monitor response to therapy, results in delayed therapeutic decision making. This not only allows, but often depends on, progression of disease for decision making, to the detriment of the patient.

We have previously used NLOM to describe normal and pathological alterations of articular cartilage.[19] NLOM provides images with very high resolution at depths of up to 800 μm in soft tissues,[20] and this can be increased by several hundred microns when using extrinsic stains. Tissue pathology characteristics of RA occur within a depth of 100 μm of the synovial surface,[21–23] which is well within the capabilities of NLOM.

NLOM presents a potential alternative for high resolution, minimally invasive *in vivo* imaging for early detection and serial monitoring of response to therapy in patients with inflammatory joint disease. The hypothesis for this study was that NLOM could utilize the natural intrinsic fluorescence properties of tissue to generate images that would allow visualization of the distinguishing structural and cellular characteristics of normal and pathologic synovial tissue in fresh, unfixed tissue specimens. To test this hypothesis, fresh, unstained normal and induced pathologic rabbit joint tissue representing two very different forms of inflammatory joint disease was imaged by NLOM and compared to standard hemotoxylin and eosin (HE) histology.

Comparison of high resolution NLOM images to histology of the same joint tissue specimens obtained from normal and standard rabbit models of induced immune-mediated and inflammatory joint disease demonstrated the ability of NLOM imaging to reveal the same characteristics of structural and cellular composition, as were observed in the HE stained histology sections. This technology produces high resolution images of synovial tissue that demonstrate characteristics of normal and different pathologic processes without the need for tissue biopsy and processing. This suggests that NLOM might be an important tool for the minimally invasive study, early diagnosis, and monitoring of therapy in inflammatory and degenerative joint diseases, where the limitations of current imaging technologies allows the progression of disease before important therapeutic decisions can be made.

2 Materials and Methods

2.1 *Normal Synovium*

Specimens of normal synovial tissue for histology and NLOM imaging were obtained from New Zealand white rabbits weighing 4 to 5 Kg that were terminated under Institutional Animal Care and Use Committee (IACUC)-approved projects performed in other laboratories where the knee joints were not affected.

2.2 *Animal Injection Preparation*

New Zealand white rabbits (Western Oregon Rabbit Company, Philomath, Oregon) weighing ~4 Kg were used in the research study, which was approved by the IACUC of the University of California, Irvine. Prior to intra-articular injection of an experimental agent, rabbits were immobilized with an intramuscular injection of 25-mg/Kg ketamine HCl. Following immobilization, 2 to 5% isoflurane was administered via face mask throughout the preparation of the inoculation site, the placement of the fentanyl patch, and during intra-articular injection. The injection site was shaved and sterilized using a chlorhexidine acetate scrub, cleaned with alcohol, and sprayed with 2% chlorhexidine acetate solution. An intra-articular injection of the experimental agent was made into the knee joint by inserting a 25-gauge needle into the joint space from the lateral aspect through a window identified by palpation of the lateral margin of the patella, the proximal lateral margin of the tibia, and the cranio-distal margin of the lateral femoral condyle.

For relief of anticipated knee pain a transdermal fentanyl patch (25 μg/h) (Mylan Pharmaceuticals Incorporated, Morgantown, West Virginia) was applied to freshly shaved skin on the dorsum in the intrascapular region.[24] Fentanyl patches were removed and replaced every 4 days. Each new patch was applied to an adjacent freshly shaved area of the dorsal intrascapular region.

2.3 *Lipopolysaccharide-Induced Arthritis Model*

Arthritis of an immune-mediated etiology was induced in a standard rabbit model using two intra-articular injections of 50-μg lipopolysaccharide from *E. coli* 0111, B4 (L5293, Sigma Chemical Company, Saint Louis, Missouri) suspended in 0.1 ml of sterile saline.[25] Three animals received an injection of LPS in the right knee on day 0 and again on day 4, and then one animal each was euthanized and tissue harvested on days 4, 11, and 18.

2.4 *Septic Arthritis Model*

Septic arthritis was induced in a standard rabbit model[26,27] using one intra-articular injection of penicillin-sensitive *Staphylococcus aureus* (ATCC 25923) (American Type Culture Collection, Rockville, Maryland) maintained and prepared by the Department of Pathology, College of Health Sciences at the University of California, Irvine. A single injection of a bacterial inoculum titrated to 10^4 colony forming units/ml sterile saline and 0.1 ml (10^3 CFU) was made into the right knee of each of the three rabbits in the same manner as the injection procedure described for the LPS model. The day of injection was designated day 0, and one animal each was euthanized and tissue harvested on days 2, 4, and 8 postinjection.

2.5 *Specimen Collection and Preparation*

Rabbit models have been used extensively in human joint disease research because of the similarities that exist in pathology and pathogenesis, and the ease with which the relatively large rabbit knee joint can be studied in contrast to the mouse joint. In this study, within three hours following euthanasia, synovium was obtained from the knee joints of 12 normal adult male New Zealand white rabbits and three treated rabbits in each of two induced arthritis groups.

Harvested rabbit knee joints were dissected on the medial and lateral aspects to expose each meniscus, and a tissue specimen was obtained from each side of the joint, providing a total of two tissue specimens from each joint. The meniscus was lifted from the tibial surface and both the meniscus and the attached joint capsule were removed from each side of the joint without changing the shape or size of the synovial mem-

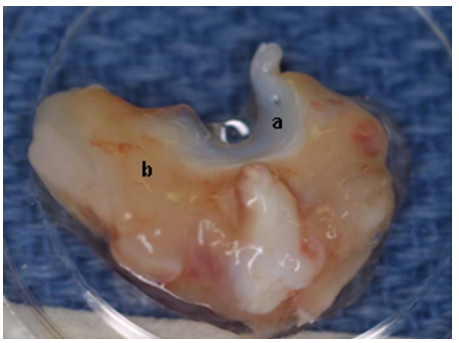

Fig. 3 (a) Meniscus with (b) synovium covered joint capsule attached to its lateral margin, as dissected from a rabbit knee joint. Retention of the meniscus allowed orientation and easy manipulation of the joint capsule tissue without disrupting the synovium.

brane. Each meniscus remained attached to the joint capsule adjacent to it so that the tissue could be manipulated without disrupting the synovium (Fig. 3), and so that the inner surface of the joint capsule where the synovium is located could always be identified. The synovial lining obtained from the site of attachment to the meniscus is adipose synovium. Each specimen was approximately 15×15 mm.

Each sample of adipose synovium was placed in a fluorescence microscopy dish (Fluorodish, World Precision Instruments, Incorporated, Sarasota, Florida) containing a drop of 0.9% saline solution to maintain tissue hydration. As the NLOM imaging system uses an inverted microscope, the synovium, which is on the inside surface of the joint capsule, was carefully placed face-down flat, without any gross folds or under any tension, on the bottom of the microscopy dish, and imaging signals were collected in the backward direction. The specimen was covered with a piece of saline-soaked gauze to further prevent dehydration during imaging. Each microscopy dish with a synovium sample was stored in a sealed bag at 4 °C until imaged. All samples were imaged within 3 h of collection except for one normal specimen that was imaged 25 h after collection.

2.6 *Histology*

Following NLOM imaging, each specimen was fixed in 10% buffered formalin at room temperature for 12 h, and then rinsed and stored in phosphate-buffered saline solution. Each specimen was subsequently dehydrated, cleared, imbedded in paraffin, cut into 6-μm-thick sections, and placed onto slides. The mounted slide sections were deparaffinized and the slide preparations stained with H&E (Sigma-Aldrich, Saint Louis, Missouri).

The stained slide sections were imaged using light microscopy (Olympus BH-2, Olympus America, Incorporated, Melville, New York) and a MicroFire digital imaging system (Olympus America, Incorporated) coupled to a computer and recorded using image capture software (PictureFrame, Optronics, Goleta, California). Synovial images from light microscopy were then compared to NLOM images to define the structures and cells imaged within each specimen.

2.7 *Nonlinear Optical Microscopy*

NLOM was performed using a Zeiss LSM 510 NLO Meta system (Carl Zeiss MicroImaging, Incorporated, Thornwood, New York) with a Coherent Chameleon Ti:sapphire femtosecond laser (Coherent, Incorporated, Santa Clara, California) as the excitation source. The Chameleon laser source provided 140-fs pulses at a repetition rate of 80 MHz, with the center frequency tunable from 690 to 1040 nm. Excitation wavelengths of both 730 and 800 nm were used in this study, as they induce an optimal combination of imaging signals from intracellular compounds and collagen, respectively.[10,15,28]

While using 800-nm excitation, light emission from the tissue was separated into two channels using the grating-based Meta detector available in the Zeiss LSM 510 NLO system. The channel containing SHG emission between 395 and 405 nm is pseudocolored blue, while the channel containing TPF emission in the range 415 to 600 nm is pseudocolored green. The TPF signal was collected over a relatively wide bandwidth (185 nm), as the sources of TPF are numerous biomolecules with different emission peaks[10] and distinct TPF spectra within that bandwidth. Excitation at 730 nm elicited a stronger TPF but much weaker SHG signal than was observed with the 800-nm wavelength. The TPF signal collected from the tissue following 730-nm excitation was divided into two channels to enhance contrast using a bandpass filter (390 to 465 nm), and using the Meta detector (470 to 650 nm). These channels were pseudocolored turquoise (390 to 465 nm) and orange (470 to 650 nm). The turquoise channel contains fluorescence mainly from mitochondrial NADH, and some other intrinsic fluorophores like folic acid and retinol that have fluorescence peaks within the 390- to 465-nm bandwidth. The orange channel collected fluorescence from riboflavin and other biomolecules with fluorescence peaks beyond 500 nm.[10]

As our purpose was to image synovium in its native state, no fluorescent stains were used on the tissue. To thoroughly survey each tissue specimen, images were obtained from: 1. the meniscus-synovium interface, 2. the central region of the synovial specimen, and 3. the region along the periphery where the adipose synovium attaches to articular cartilage. These imaging regions were 3 to 5 mm apart. The imaging region at the periphery was chosen such that it was at least 2 mm from the cuts made during sample extraction.

Images 512×512 pixels and 1024×1024 pixels of tissue areas from 225×225 μm to 2.25×2.25 mm were obtained using 20×, 0.45-NA and water immersion 40×, 0.8-NA objectives. To image an area 1.125×1.125 mm or larger, individual adjacent 225×225-μm images were acquired sequentially and combined to form the larger image. This technique, known as "tiling," allows construction of a large, clear geographical image of the synovial tissue (Fig. 4). NLOM imaging scan speeds from 6.5 to 102 μsec per pixel were evaluated. The combination of a 40×, water immersion objective (Achroplan, 0.8 NA) delivering 20 mW at the tissue surface and a pixel dwell time of 6.5 μsec provided images with sufficient cellular detail without thermally damaging the tissue, even during the relatively long time (7 to 15 min) required to acquire a stack of up to 70 images from the same location in successive planes at 1-μm intervals. The minimum power required for image acquisition was 18 mW de-

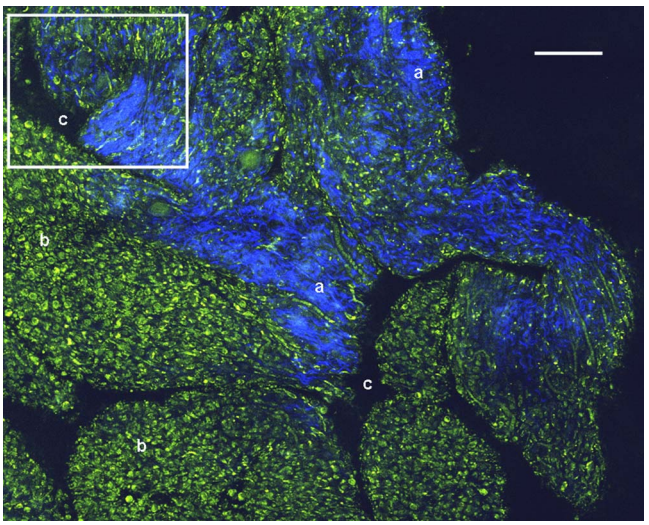

Fig. 4 A NLOM tiled image of the synovial surface layer constructed from sequentially acquired 225 × 225-μm images using 800-nm excitation. (a) The SHG emission from collagen is in blue, (b) TPF, in green, is mostly from intracellular sources, and (c) spaces between synovial folds lack any fluorescence signal. Scale bar is 100 μm. The box-enclosed area is further magnified in Fig. 8(A) to show cellular details. (Color online only.)

livered to the sample with a pixel dwell time of 6.5 μs. Below that level, the emission signals were judged to be too weak for imaging. Power levels above 34 mW used with a pixel dwell time of 12.8 μs caused tissue damage.

2-D images as well as 3-D tomographic stacks of individual 2-D images obtained at 1- to 2-μm intervals to a depth of up to 70 μm, referred to as Z stacks, were obtained to study tissue morphology in successive image planes within a volume of tissue (Fig. 2).

3 Results

3.1 *Histology*

An HE stained histology preparation of adipose synovium from the normal knee joint of a rabbit is shown in Figs. 5(A) and 6(A). The cross section of synovium demonstrates both intima and subintima. The sharp transition between the intima and subintima and the characteristic morphological details of each of these layers of adipose-type synovium are easily observed. The intima is seen as a densely populated cellular region that is one to three cells thick, while the subintima is composed primarily of adipocytes and small numbers of capillaries, small venules, and arterioles set in a randomly distributed matrix of loosely packed thin collagen fibrils.

The three animal subjects in the septic arthritis group demonstrated a polymorponuclear inflammatory response with loss of normal intimal and subintimal morphology as anticipated, which was progressive with increasing time from joint inoculation, and could be characterized in both NLOM and HE stained histology sections. The image of the HE stained histologic section of the adipose synovium of the rabbit knee at 8 days following inoculation with *S. aureus* [Fig. 5(B)] represents the most advanced septic pathology of the study, and reveals an inflammatory reaction with a denuded intimal surface and a thickened and edematous subintima. The adipocytes found in normal adipose synovium have been replaced by an inflammatory cell infiltrate consisting primarily of heterophils. Capillaries are congested and their walls are thickened. The meshwork of pre-existing collagen fibers is randomly displaced and fibroblasts produce a delicate fibrillar matrix.

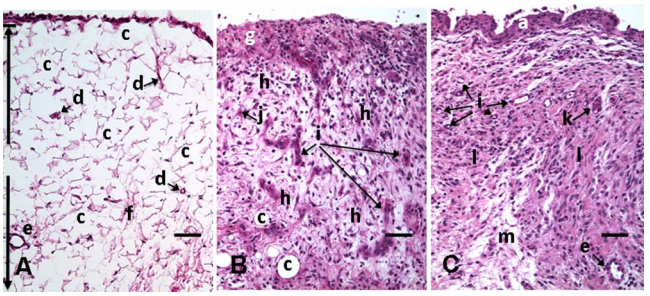

Fig. 5 HE stained histological images of adipose synovium from (A) a knee joint of a normal rabbit, (B) 8 days postinoculation with *S. aureus,* and (C) 18 days postinoculation with LPS from *E. coli.* (A) In the cross section of normal adipose synovium, the intima (a) is seen as a densely populated cellular region that is one to three cells thick, while the subintima (b) is composed primarily of adipocytes (c) and small numbers of capillaries (d), small venules (e), and arterioles set in a randomly distributed matrix of loosely packed thin collagen fibrils (f). The sharp transition between the intima and subintima and the characteristic morphological details of each layer are easily observed. The cross section of adipose synovium from the *S. aureus* infected knee (B) demonstrates that a denuded intimal layer (g) and the adipocytes (c) of the thickened and edematous subintima have been largely replaced by an inflammatory cell infiltrate (h) consisting primarily of heterophils. Capillaries (i) are congested and their walls are thickened. Fibroblasts (j) are beginning to produce a delicate fibrillar matrix, while the meshwork of pre-existing collagen fibers is randomly displaced. The image of the inflammatory reaction that is present in the adipose synovium of the rabbit knee joint following LPS inoculation (C) demonstrates thickening of the intimal layer (a), and the normal population of subintimal adipocytes has been replaced by an inflammatory cell infiltrate (l) consisting primarily of lymphocytes relatively evenly distributed, along with fibroblasts in a collagenous matrix containing congested capillaries (i), arterioles (k), and venules (e). In some areas, edema (m) separates the matrix of collagen fibrils. Scale bars are 50 μm.

The three animal subjects in the LPS arthritis group demonstrated intimal thickening with a mononuclear inflammatory response that was progressive with increasing time from joint inoculation, the characteristics of which could be distinguished in both NLOM images and HE stained histology sections. A photomicrograph of an HE stained histology section of the inflammatory reaction that is present in adipose synovium of the rabbit knee 18 days after LPS inoculation [Fig. 5(C)] represents the most advanced immune-mediated pathology of the study, and demonstrates a thickened intima. The normal population of adipocytes has been replaced by an inflammatory cellular infiltrate consisting primarily of lymphocytes evenly distributed along with fibroblasts in a collagenous matrix. The matrix also contains congested capillaries, arterioles, and venules that in some areas are separated by edema.

3.2 *Nonlinear Optical Microscopy Imaging of Synovium*

Figure 4 demonstrates a typical NLOM image of the synovial surface layer using 800-nm excitation and a scan rate of

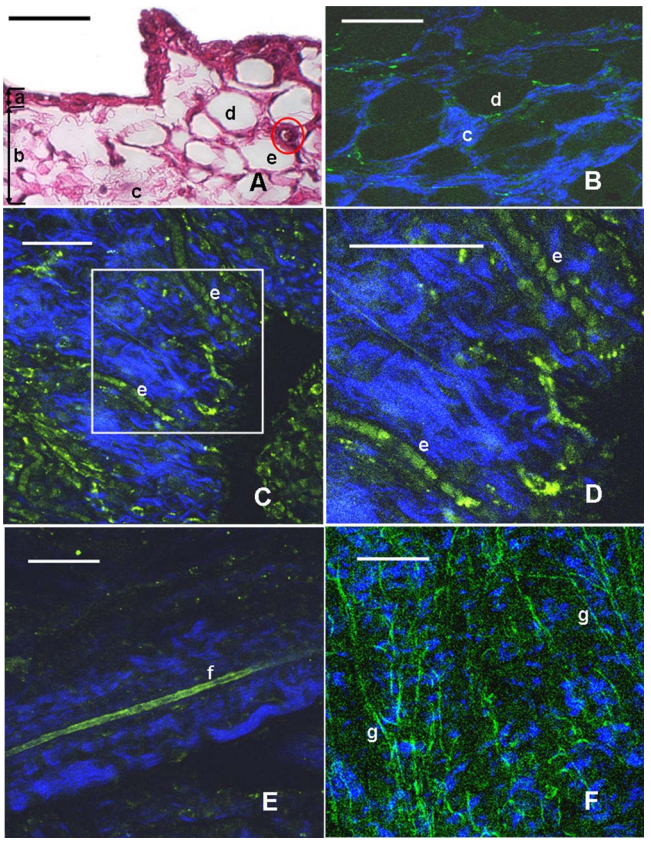

Fig. 6 Important synovial structures as demonstrated by (A) HE sectioning and (B) through (F) NLOM imaging using 800-nm excitation. All images except for (D) are presented in the same scale for ease of comparison. The HE section shows the thin intimal layer (a) and the much thicker subintima (b). Collagen (c) appears as a widespread wavy pattern in (A) and is identified particularly well by its strong blue SHG signature in (B) through (F). Adipocytes (d) appear as empty spaces in the extracellular collagen matrix in the HE stained section (A) and as dark oval structures enclosed by the blue SHG signal of the collagen fibers in the NLOM image (B). Rouleaux formation of erythrocytes in undulating venuoles (e) set in a background meshwork of blue collagen fibrils of the subintima are seen in (C) and (D). (D) Image is a magnification of the area inside the box in (C), and demonstrates the visualization of individual erythrocytes. An arteriole (f) is seen in (A) and in (E), where the green colored TPF signal of elastin fibers outline the wall of a linearly oriented arteriole. Arteriole walls have elastin that provides a strong TPF signal, while the primarily collagen-containing venule walls produce only a SHG signal that highlights erythrocytes within the vascular lumen (e). Linearly directed elastin fibers appearing as green filaments (g) set in a meshwork of less-well-oriented blue collagen fibers are observed in synovial tissue along the insertion line of the adipose synovium with the meniscus (F). Scale bars are 50 μm for all images. (Color online only.)

12.8 μsec per pixel. The SHG (blue) signal reveals the dense matrix of collagen and the TPF (green) signal from intracellular compounds highlights individual cells. NLOM imaging of cells and tissues was not affected by periods of tissue storage that ranged from 3 to 25-h postdissection.

The imaging signals from the tissue showed quadratic dependence on excitation intensity as expected for TPF and SHG sources. The tissue emission spectra measured in the spectral imaging mode of the Zeiss LSM 510 NLO Meta system helped further characterize the nature of the SHG signal.

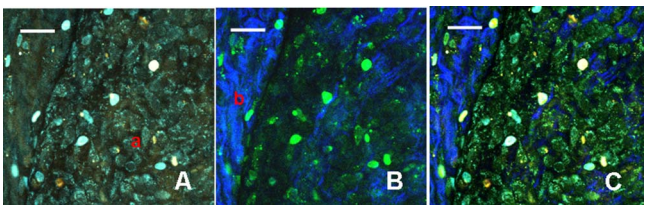

Fig. 7 Comparison of synovial images of the same location acquired using (A) 730-nm excitation and (B) 800-nm excitation at a pixel dwell time of 12.8 μsec. At this scan speed, cells (a) appear clearer with 730-nm excitation, while collagen (b) is most clearly distinguished when using 800-nm excitation. (C) An improved image was created by combining the TPF channels from (A) and SHG channel from (B). Scale bars are 20 μm.

For different wavelengths of excitation, the sharp SHG peak always occurred at exactly half the incident wavelength, as anticipated. With no correction for the spectral dependence of optical component performance, the SHG signal from extracellular collagen weakened and the TPF from tissue constituents brightened as the excitation wavelength was decreased from 800 to 730 nm. This is consistent with NLOM imaging of other tissues.[10,28]

When using 800-nm excitation, the use of slow scan speeds corresponding to pixel dwell times of 12.8 and 25.6 μsec were found to provide sufficient signal collection at each pixel to produce bright, clear images. In Figs. 6(C) and 6(D), where a dwell time of 12.8 μsec per pixel was used, individual erythrocytes within blood vessels [Fig. 6, part e] are clearly visible. When the scan speed is increased on the same tissue sample, erythrocytes lose clear definition and become difficult to identify. The problem with using slow scan speeds, however, is the potential for thermal injury to the tissue.

Excitation with 730 nm [Fig. 7(A)] produced clear images of cells at faster scan speeds (pixel dwell times of 6.4 to 12.8 μsec per pixel); however, the collagen signal was very weak. When using an 800-nm incident beam at these higher scan speeds [Fig. 7(B)], collagen still produced a clean, bright SHG signal, as reported previously.[28] A combination of the TPF channels from the 730-nm excitation image [Fig. 7(A)] and the SHG channel from the 800-nm excitation image [Fig. 7(B)] is shown in Fig. 7(C). Combining separate images obtained from 730- and 800-nm excitation wavelengths provided the sharpest and most detailed image of cellular and collagen composition of the tissue specimen.

3.3 *Identification of Morphologic Characteristics of Normal Synovial Tissue*

A number of structures of normal synovium were clearly identified by NLOM imaging. Adipocytes are seen in the NLOM image in Fig. 6(B) as large ovoid black spaces with their cell margins marked by a TPF signal, surrounded by collagen fibers identified by their characteristic SHG signal. Adipocytes appear dark in NLOM due to the large volume of lipid content, which does not fluoresce. The adipocytes [Fig. 6, part d] of the NLOM image [Fig. 6(B)] are comparable in size and morphology to those demonstrated in HE preparations [Fig. 6(A)].

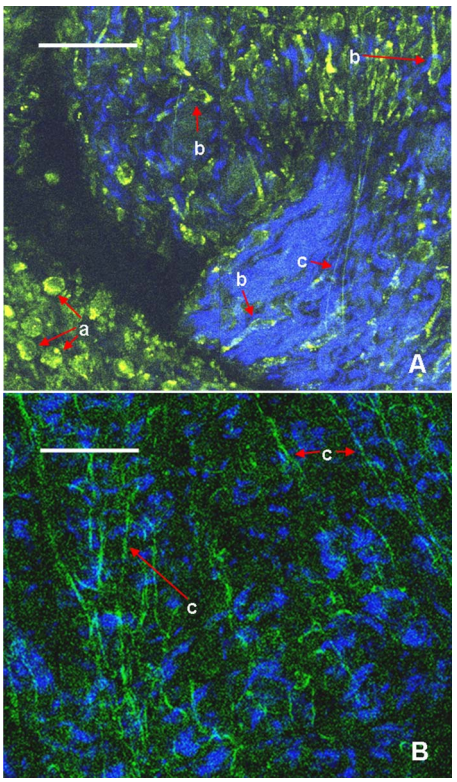

Fig. 8 Magnified NLOM images showing synovial cells and elastin fibers from (A) the box-enclosed area of Fig. 4, and (B) from Fig. 6(F). Rounded synoviocytes, 10 to 20 μm in diameter (a), and elongated synoviocytes, 40 to 50 μm long (b), can be distinguished in (A). Long, thin elastin-like fibers (c) in (A) and (B) are observed to be morphologically distinct from the elongated synoviocytes in (A). Scale bars are 50 μm.

NLOM demonstrated both venules and arterioles in synovium [Figs. 6(C)–6(E)]. Venule walls, which contain collagen, emitted an SHG signal, while the erythrocytes within the lumen emitted a TPF signal. The two signals produced sufficient contrast to clearly identify erythrocytes inside the venules [Fig. 6(D)]. On the other hand, arteriolar walls contain a high concentration of elastin, which emits a strong TPF signal.[10] The overlapping TPF signals emitted both from erythrocytes and the elastin in arteriole walls made it difficult to identify individual erythrocytes within arterioles [Fig. 6(E)].

Variable-length, 1 to 2 μm wide, TPF-emitting filamentous strands typical of elastin[10] were observed in the subintima of the synovium, generally in association with the dense collagen matrix, in regions adjacent to the attachment of the joint capsule to bone [Figs. 6(F), 8(A), and 8(B)]. The elastin fibers were not highly organized but do appear to have some common directionality in the regions where they are present. While the elastin fibers were clearly observed where they lie in a longitudinal orientation to the imaging plane, because of their narrow diameter, it is possible that their presence was not recognized where they lie perpendicular to the imaging plane.

Cells were identified by the green fluorescence from their cytoplasm silhouetting dark nuclei, as seen in Fig. 8(A) (a magnified view of the boxed region in Fig. 4). Figure 8(A) demonstrates cells of different morphologies imaged in synovial tissue by NLOM. Synoviocytes in HE sections only demonstrated an oval morphology, while NLOM imaging [Fig. 8(A)] allowed identification of both round [Fig. 8, part a] and elongated [Fig. 8, part b] synoviocytes as well as the collagen matrix (blue).

Images with structural detail of tissue could be obtained to a depth of 70 μm from the synovial surface. Image stacks of normal adipose-type synovium acquired using 730-nm excitation clearly demonstrate the structural distinction between the intima and subintima. The dense layer of cells within the intima produces a strong TPF signal, while the loosely collagenous matrix of the subintima that has poor SHG initiation at 730 nm remains relatively dark. The depth at which there is a transition from intima to subintima could be determined by viewing successive image planes from a Z stack for an abrupt change in cellular and matrix composition.

3.4 *Identification of Morphologic Characteristics of Pathologic Synovial Tissue*

All NLOM images of septic inflammatory and LPS-induced synovitis tissue demonstrated increased cellular content when compared to normal tissue at equivalent locations and depths (Figs. 9 and 10). This was particularly evident in areas below the intimal layer, where normal subintimal tissue has substantially fewer cells than the intima. Histologic sections of the pathology specimens demonstrated a marked inflammatory response characterized by mixed inflammatory cells, macrophages and fibroblasts in the septic specimens [Fig. 9(D)], and a generalized and predominantly lymphocytic infiltration with pronounced intimal thickening observed in the synovium of the LPS-treated joints [Fig. 9(G)]. NLOM images of LPS and septic specimens revealed increased intracellular fluorescence consistent with the elevated level of metabolic activity of cells actively engaged in the inflammatory response [Figs. 9(E), 9(F), 9(H), and 9(I)]. There was a conspicuous absence of collagen SHG observed in the septic tissue [Figs. 9(F) and 10(C)], while collagen SHG, although reduced, continued to be observed in synovial tissue of the LPS-treated joints [Figs. 9(I) and 10(D)]. The larger size of the inflammatory cell types (heterophils and macrophages) with lobulated nuclei, and the elongated morphology of the fibroblasts was clearly evident in the NLOM images of the septic tissue [Figs. 9(E), 9(F), and 10(C)], while lymphocytes that are morphologically smaller in size with an oval nucleus, with minimal to no evidence of fibroblast activity, and the continued observation of some collagen SHG characterized the pathology of the tissue from LPS-treated joints [Figs. 9(H), 9(I), and 10(D)].

4 Discussion

By utilizing intrinsic tissue TPF and SHG, NLOM is able to produce vivid images of synovium without the need of tissue fixation, sectioning, and staining. Cells, blood vessels, and tissue matrix components such as collagen and elastin can be readily identified in fresh, unfixed tissue by NLOM imaging. The characteristic undulating structure of the synovial surface is observed (Fig. 4), where the green fluorescing intimal cells and blue fluorescing collagen of the subintima reveal components of the tissue, while the dark regions represent adipocytes or spaces between tissue folds that can be easily differ-

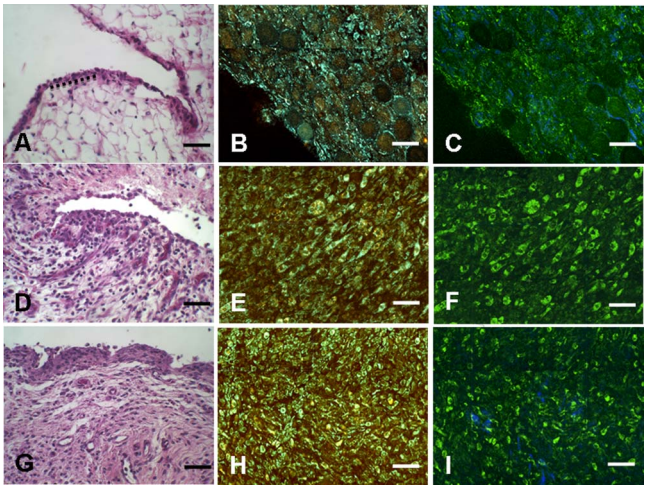

Fig. 9 Images of rabbit synovial tissue, (A), (B), and (C) normal, (D), (E), and (F) 8 days postbacterial inoculation, and (G), (H), and (I) 18 days post-LPS intra-articular injection, demonstrating HE stained histology sections in (A), (D), and (G), NLOM using 730-nm excitation in (B), (E), and (H), and NLOM using 800-nm excitation in (C), (F), and (I). All NLOM images were acquired in a plane parallel to and at a depth of 15 μm from the specimen surface [dotted line, in (A)] and thus primarily image the inflammatory response within the intima. Histologic sections of the pathology specimens demonstrate a marked inflammatory response characterized by mixed inflammatory cells, macrophages, and fibroblasts in the septic specimens in (D) and a generalized and predominantly lymphocytic infiltration with pronounced intimal thickening observed in the synovium of the LPS-treated joints in (G). NLOM images of both pathology specimens in (E), (F), (H), and (I) reveal increased intracellular fluorescence consistent with the elevated level of metabolic activity of cells actively engaged in the inflammatory response. There is a conspicuous absence of collagen SHG observed in the septic tissue in (F), while collagen SHG (blue) continues to be observed in synovial tissue of the LPS-treated joints in (I). The larger size of the inflammatory cell types (heterophils and macrophages) with multilobulated nuclei and the elongated morphology of the fibroblasts is clearly evident in the NLOM images of the septic tissue in (E) and (F), while in lymphocytes that are morphologically smaller in size with an oval nucleus, minimal to no evidence of fibroblast activity and the continued observation of some collagen SHG characterize the pathology of the tissue from LPS-treated joints in (H) and (I). Scale bars are 50 μm. (Color online only.)

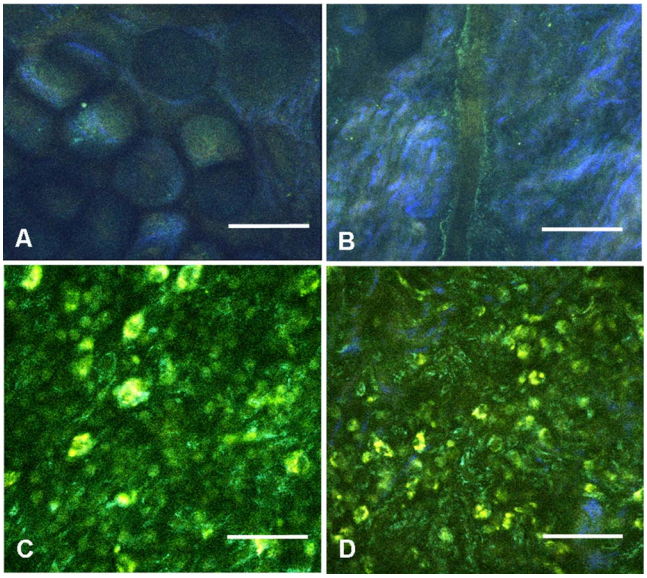

Fig. 10 NLOM images of rabbit synovial tissue demonstrating the enhanced image quality achieved by combining images acquired by sequential 730-nm and then 800-nm excitation. The images illustrated were obtained from the subintima in a plane parallel to and at a depth of 45 μm from the surface of (A) and (B) normal, (C) 8 days postbacterial inoculation, and (D) 18 days post-LPS intra-articular injection specimens. At a depth of 45 μm, the imaging plane is below the intimal layer of the normal synovium and demonstrates subintimal tissue predominately consisting of (A) adipocytes or (B) collagen matrix with little other cellular content, while both the (C) septic and (D) LPS specimens demonstrate a substantial increase in cellular content consistent with the inflammatory processes. The septic tissue demonstrates large cells with multilobular nuclei characteristic of rabbit heterophils and macrophages, along with elongated cells characteristic of fibroblasts, while the cellular infiltrate observed in the LPS specimens are smaller cells with oval nuclei characteristic of an inflammatory response predominated by lymphocytes. SHG emission of collagen, viewed as blue fibrils in the NLOM images, is not observed in the subintimal tissue of the septic specimens in (C), while it continues to be observed, although in reduced amounts, in LPS specimens in (D). Scale bars are 50 μm. (Color online only.)

entiated. Intrinsic spectral signatures of many biological molecules have been reported, and these signatures can be used to recognize the presence or absence of biomolecules in a tissue sample using NLOM.[10]

In this study, the cell cytoplasm provided intrinsic TPF emission with either 730- or 800-nm excitation. The TPF emission is retained within the boundary of the cell wall and surrounds the nucleus, which appears in dark silhouette. This permits the observation of individual cells within the tissue and assists with characterization of the morphology of the nucleus. At 800-nm excitation, collagen produced a strong SHG signal. This behavior is consistent with observations reported for other tissue.[28]

Excitation at 730 nm induced much brighter TPF from synovial tissue than did excitation at 800 nm for the same excitation power. When using 730-nm excitation, red blood cells (RBCs) showed relatively strong fluorescence in the 490- to 650-nm channel compared with other cells. When acquiring stacks of images from successive depths at a single location, excitation at 730 nm reduces the chance of causing thermal injury to the tissue, because lower excitation power can be used to acquire individual images.

This study demonstrated that NLOM is able to image synovium with definition of structural and cellular components with resolution similar to histologic sectioning. NLOM imaging allowed visualization of synoviocytes, arterioles, venules, collagen, and elastin that are important for the routine characterization of normal and pathologic tissue specimens. Additionally, imaging of pathologic synovial tissue demonstrated the ability to visualize the increased cellular content and reduction in normal collagen content of the intimal and subintimal layers of diseased synovial tissue, and discern characteristics of heterophils, macrophages, lymphocytes, and fibroblasts that are specific to different inflammatory processes. Despite the presence of some fibroblasts and fine fibrillar elements, there is a substantial reduction in the synovial SHG signal observed in the diseased specimens, as seen in Figs. 9 and 10. This may be due to inflammatory cellular infiltrates and edema displacement of the collagen matrix.

More likely, the decreased SHG signal in the disease specimens is due to: 1. breakdown of the collagen matrix by cytokines and other inflammatory products, and/or 2. fibroblast generation of procollagen fibrils in tissue repair that have yet to be organized into fibers with the SHG-emitting intensity that is detectable with the imaging dwell times used in this study.

Establishing a definitive diagnosis of joint disease currently requires evaluation of patient history and examination, laboratory tests, and the histologic examination of synovial tissue biopsy obtained by closed needle[29] or athroscopic[30] techniques. In this study we have demonstrated that NLOM is able to acquire high-resolution images to a depth of 70 μm, which should be sufficient to visualize pathologic changes in synovium associated with inflammatory joint disease.[21–23]

Using standard light microscopy to study synovial structure and pathology requires biopsy, processing, sectioning, and staining of tissue specimens, while NLOM permits synovial imaging without biopsy and histology processing. As NLOM typically produces a tangential (horizontal) cross sectional plane of view instead of the transverse (vertical) cross sectional plane generally associated with standard histology sections, adaptation to the tangential orientation by the clinician or pathologist will be necessary. The Z stack modality of image acquisition and visualization provides a series of successive single images of the tissue microstructure and composition from the synovial surface to a depth of about 70 μm, which enhances the ability to determine intimal thickness and depth of synovial structures, as is commonly observed in the classic histologic orientation. Visualizing tissue depth *in situ* using NLOM should permit almost real-time imaging and evaluation of intimal hypertrophy, vascular proliferation, cellular infiltration, and other pathologic changes in a depth-resolved image.

This study demonstrates that NLOM is able to provide high-resolution images of normal synovial tissue and synovial tissue from animal models of septic and LPS-induced immune-mediated joint disease, and suggests that *in vivo* NLOM imaging may be a useful alternative to routine joint biopsy. The use of NLOM to identify tissue changes associated with disease will require further investigation and validation, particularly in its ability to differentiate and characterize cell types associated with pathology in specimens of naturally occurring disease.

For clinical application, NLOM will need to be adapted for minimally invasive arthroscopic procedures. This will require development of an endoscopic probe that is less than 2 mm in diameter and about 10 cm long that can be passed through an insertion needle or used with a standard arthroscope. Imaging resolution with the probe will need to be on the order of 1 μm to identify cell morphology characteristic of different forms of immune-mediated and inflammatory arthritis.

Gradient index (GRIN) lens-based probes[31] and scanning fiber endoscopes[32] might be possible approaches to probe design. The need for a thin endoscopic probe likely will necessitate that the scanning system be placed outside the probe rather than at the insertion tip. Other critical issues in the design of intrinsic fluorescence-based NLOM arthroscopy would be the delivery of high energy femtosecond pulses to the tissue without dispersion, and focusing these pulses through miniature high NA lenses.[33]

Delivery of femtosecond laser pulses through photonic crystal optical fibers has been demonstrated[34] and could facilitate the development of NLOM arthroscopy. The use of high pulse energies from regenerative amplifiers[35] or lower pulse durations[36] substantially increases intrinsic fluorescence generation. Also, the use of photon counting detectors will improve system sensitivity at the low signal levels that will be encountered with intrinsic TPF- and SHG-based NLOM arthroscopy.[37]

The successful imaging of synovial tissue using NLOM as reported here introduces this novel imaging modality as a potential tool for morphologic studies of inflammatory joint disease. With needle arthroscopic adaptation of this technology, it may be possible to use NLOM to evaluate the synovium of patients in a rheumatologist's office. Additionally, this technique would reduce tissue sampling artifacts that are inherent in random serial biopsies.

NLOM has potential for use in the early diagnosis of joint disease. With the recent introduction of a large number of biologic therapies,[38–40] NLOM should facilitate the *in vivo* evaluation of histologic tissue changes over a wide synovial surface area, and allow comparison of clinical response and pathologic changes in synovium in both clinical trials and practice. The further evaluation of this novel imaging technique for imaging pathologic synovial tissue in different stages of arthritis and for recognizing the early stages of joint disease is warranted.

Acknowledgments

This work was supported by the U.S. Air Force Office of Scientific Research, Medical Free-Electron Laser Program (FA9550-04-1-0101), National Center for Research Resources of the National Institutes of Health (Laser Microbeam and Medical Program, RR-01192) and the Arnold and Mabel Beckman Foundation. The U.S. Government is authorized to reproduce and distribute reprints for Governmental purposes notwithstanding any copyright notation. The views and conclusions contained herein are those of the authors and should not be interpreted as necessarily representing the official policies or endorsements, either expressed or implied, of the Air Force Research Laboratory or the U.S. Government. The schematic depictions of diarthrodial joint structure [Fig. 1(a)] and the layered structure of synovium [Fig. 1(b)] are used with permission from MedicineNet.com and Elsevier Limited, respectively.

References

1. C. G. Helmick, D. T. Felson, R. C. Lawrence, S. Gabriel, R. Hirsch, C. K. Kwoh, M. H. Liang, H. M. Kremers, M. D. Mayes, P. A. Merkel, S. R. Pillemer, J. D. Reveille, and J. H. Stone, "Estimates of the prevalence of arthritis and other rheumatic conditions in the United States. Part I," *Arthritis Rheum.* **58**, 15–25 (2008).
2. R. C. Lawrence, D. T. Felson, C. G. Helmick, L. M. Arnold, H. Choi, R. A. Deyo, S. Gabriel, R. Hirsch, M. C. Hochberg, G. G. Hunder, J. M. Jordan, J. N. Katz, H. M. Kremers, and F. Wolfe, "Estimates of the prevalence of arthritis and other rheumatic conditions in the United States. Part II," *Arthritis Rheum.* **58**, 26–35 (2008).
3. D. M. Gerlag and P. P. Tak, "Synovial fluid analysis, synovial biopsy, and synovial pathology," in *Kelly's Textbook of Rheumatology*, S. Ruddy, E. D. Harris, and C. B. Sledge, Eds., pp. 675–691, W. B. Saunders Co., Philadelphia, PA (2001).

4. D. M. Lee, G. P. Kiener, and M. B. Brenner, "Synoviocytes," in *Kelly's Textbook of Rheumatology*, S. Ruddy, E. D. Harris, and C. B. Sledge, Eds., pp. 175–188, W. B. Saunders Co., Philadelphia, PA (2001).
5. J. C. W. Edwards, "The nature and origins of synovium: experimental approaches to the study of synoviocyte differentiation," *J. Anat.* **184**, 493–501 (1994).
6. F. N. Ghadially, *Fine Structure of Synovial Joints: A Text and Atlas of the Ultrastructure of Normal and Pathological Articular Tissue*, pp. 1–41, Butterworths, London (1983).
7. C. W. Castor, "The microscopic structure of normal human synovial tissue," *Arthritis Rheum.* **3**, 140–151 (1960).
8. N. E. Shaw and B. F. Martin, "Histological and histochemical studies on mammalian knee-joint tissues," *J. Anat.* **96**, 359–373 (1962).
9. R. Bassleer, M. P. Lhoest-Gauthier, A. M. Renard, E. Heinen, and G. Goessens, "Histological structure and function of synovium," in *Articular Synovium: Anatomy, Physiology, Pathology, and Therapy. Intl. Symp. Articular Synovium*, P. Franchimont, Ed., Karger, New York (1982).
10. W. R. Zipfel, R. M. Williams, R. Christie, A. Y. Nikitin, B. T. Hyman, and W. W. Webb, "Live tissue intrinsic emission microscopy using multiphoton-excited native fluorescence and second harmonic generation," *Proc. Natl. Acad. Sci. U.S.A.* **100**, 7075–7080 (2003).
11. W. Denk, J. Strickler, and W. Webb, "Two-photon laser scanning fluorescence microscopy," *Science* **248**, 73–76 (1990).
12. I. Freund, M. Deutsch, and A. Sprecher, "Connective tissue polarity. Optical second-harmonic microscopy, crossed-beam summation, and small-angle scattering in rat-tail tendon," *Biophys. J.* **50**, 693–712 (1986).
13. V. E. Centonze and J. G. White, "Multiphoton excitation provides optical sections from deeper within scattering specimens than confocal imaging," *Biophys. J.* **75**, 2015–2024 (1998).
14. R. M. Williams, D. W. Piston, and W. W. Webb, "Two-photon molecular excitation provides intrinsic three-dimensional resolution for laser-based microscopy and microphotochemistry," *FASEB J.* **8**, 804–813 (1994).
15. W. Denk, D. W. Piston, and W. W. Webb, "Multi-photon molecular excitation in laser-scanning microscopy," in *Handbook of Biological Confocal Microscopy*, J. B. Pawley, Ed., pp. 535–545, Plenum, New York (2006).
16. P. M. Lydyard and J. C. W. Edwards, "The pathophysiology of rheumatoid arthritis," *Clin. Exp. Rheumatol.* **12**(Suppl. 11), S55–S58 (1994).
17. D. Baeten, P. Demetter, C. Cuvelier, F. Van den Bosch, E. Kruithof, N. Van Damme, G. Verbruggen, H. Mielants, E. M. Veys, and F. De Keyser, "Comparative study of the synovial histology in rheumatoid arthritis, spondyloarthropathy, and osteoarthritis: influence of disease duration and activity," *Ann. Rheum. Dis.* **59**, 945–953 (2000).
18. P. H. Curtiss, Jr, "The pathophysiology of joint infection," *Clin. Orthop. Relat. Res.* **96**, 129–135 (1973).
19. A. T. Yeh, M. J. Hammer-Wilson, D. C. Van Sickle, H. P. Benton, A. Zoumi, B. J. Tromberg, and G. M. Peavy, "Nonlinear optical microscopy of articular cartilage," *Osteoarthritis Cartilage* **13**, 345–352 (2005).
20. S. W. Teng, H. Y. Tan, J. L. Peng, H. H. Lin, K. H. Kim, W. Lo, Y. Sun, W. C. Lin, S. J. Lin, S. H. Je, P. T. C. So, and C. Y. Dong, "Multiphoton autofluorescence and second-harmonic generation imaging of the *ex vivo* porcine eye," *Invest. Ophthalmol. Visual Sci.* **47**, 1216–1224 (2006).
21. F. N. Ghadially, *Fine Structure of Synovial Joints: A Text and Atlas of the Ultrastructure of Normal and Pathological Articular Tissues*, pp. 212–235, Butterworths, London (1983).
22. D. Blake, P. Mapp, and C. R. Stevens, "The physiology of the joint and its disturbance in inflammation," in *Oxford Textbook of Rheumatology*, D. A. Isenberg, P. J. Maddison, P. Woo, D. Glass, and F. C. Breedveld, Eds, pp. 350–360, Oxford, New York (2004).
23. B. Bresnihan and P. P. Tak, "Synovial pathology," in *Oxford Textbook of Rheumatology*, D. A. Isenberg, P. J. Maddison, P. Woo, D. Glass, and F. C. Breedveld, Eds., pp. 360–367, Oxford, New York (2004).
24. P. L. Foley, A. L. Henderson, E. A. Bissonette, G. R. Wimer, and S. H. Feldman, "Evaluation of fentanyl transdermal patches in rabbits: blood concentrations and physiologic response," *Comp. Med.* **51**, 239–244 (2001).
25. H. Idogawa, A. Imamura, D. Matsuo, K. Yohitake, T. Umemura, and M. Ohashi, "A monoarthritic model in rabbits induced by repeated intra-articular injections of lipopolysaccaride," *Int. J. Exp. Pathol.* **79**, 93–104 (1998).
26. P. J. Strouse, F. Londy, M. A. Di Pietro, E. L. Teo, C. E. Chrisp, and K. Doi, "MRI evaluation of infectious and non-infectious synovitis: preliminary studies in a rabbit model," *Pediatr. Radiol.* **29**, 367–371 (1991).
27. D. Daniel, W. Akeson, D. Amiel, M. Ryder, and J. Boyer, "Lavage of septic joints in rabbits: effects of chondrolysis," *J. Bone Jt. Surg., Am. Vol.* **58**, 393–395 (1976).
28. A. Zoumi, A. Yeh, and B. J. Tromberg, "Imaging cells and extracellular matrix *in vivo* by using second-harmonic generation and two-photon excited fluorescence," *Proc. Natl. Acad. Sci. U.S.A.* **99**, 11014–11019 (2002).
29. H. R. Schumacher Jr. and J. P. Kulka, "Needle biopsy of the synovial membrane—experience with the Parker-Pearson technic," *N. Engl. J. Med.* **286**, 416–419 (1972).
30. A. Zschabitz, M. Neurath, J. Grevenstein, H. Koepp, and E. Stofft, "Correlative histologic and arthroscopic evaluation in rheumatoid knee joints," *Surg. Endosc* **6**, 277–282 (1992).
31. J. C. Jung and M. J. Schnitzer, "Multiphoton endoscopy," *Opt. Lett.* **28**, 902–904 (2003).
32. C. M. Lee, C. J. Engelbrecht, T. D. Soper, F. Helmchen, and E. J. Seibel, "Scanning fiber endoscopy with highly flexible, 1 mm catheterscopes for wide-field, full-color imaging," *J. Biophoton.* **3**(5–6), 385–407 (2010).
33. R. P. J. Barretto, B. Messerschmidt, and M. J. Schnitzer, "*In vivo* fluorescence imaging with high-resolution microlenses," *Nat. Methods* **6**, 511–512 (2009).
34. W. Gobel, A. Nimmerjahn, and F. Helmchen, "Distortion-free delivery of nanojoule femtosecond pulses from a Ti:sapphire laser through a hollow-core photonic crystal fiber," *Opt. Lett.* **29**, 1285–1287 (2004).
35. P. Theer, M. T. Hasan, and W. Denk, "Two-photon imaging to a depth of 1000 micron in living brains by use of a Ti:Al2O3 regenerative amplifier," *Opt. Lett.* **28**, 1022–1024 (2003).
36. S. Tang, T. B. Krasieva, Z. Chen, G. Tempea, and B. Tromberg, "Effect of pulse duration on two-photon excited fluorescence and second harmonic generation in nonlinear optical microscopy," *J. Biomed. Opt.* **11**, 020501 (2006).
37. R. K. P. Benninger, W. J. Ashby, E. A. Ring, and D. W. Piston, "Single-photon-counting detector for increased sensitivity in two-photon laser scanning microscopy," *Opt. Lett.* **33**, 2895–2897 (2008).
38. N. J. Olson and C. M. Stein, "New drugs for rheumatoid arthritis," *N. Engl. J. Med.* **350**, 2167–2179 (2004).
39. D. E. Furst, F. C. Breedveld, J. R. Kalden, J. S. Smolen, G. R. Burmester, J. W. J. Bijlsma, M. Dougados, P. Emery, E. C. Keystone, L. Klareskog, and P. J. Mease, "Updated consensus statement on biological agents, specifically tumour necrosis factor α (TNFα) blocking agents and interleukin-1 receptor antagonist (IL-1ra), for the treatment of rheumatic diseases, 2005," *Ann. Rheum. Dis.* **64**, iv2–iv14 (2005).
40. S. B. Cohen, P. Emery, M. W. Greenwald, M. Dougados, R. A. Furie, M. C. Genovese, E. C. Keystone, J. E. Loveless, G. R. Burnmester, M. W. Cravets, E. W. Hessey, T. Shaw, M. C. Totoritis, and REFLEX Trial Group, "Rituximab for rheumatoid arthritis refractory to anti-tumor necrosis factor therapy. Results of a multicenter, randomized, double-blind, placebo-controlled, phase III trial evaluating primary efficacy and safety at twenty-four weeks," *Arthritis Rheum.* **54**, 2793–2806 (2006).